On the role of sodium and copper off-stoichiometry in Cu (In,Ga)S 2 for photovoltaic applications: Insights from the investigation of more than 500 samples

Léo Choubrac, Eugene Bertin, Fabien Pineau, Ludovic Arzel, Thomas Lepetit, Lionel Assmann, Thamer Aloui, Sylvie Harel, Nicolas Barreau

Léo Choubrac[a], Eugene Bertin[a,b], Fabien Pineau[a], Ludovic Arzel[a], Thomas Lepetit[a], Lionel Assmann[a], Thamer Aloui[a], Sylvie Harel[a], Nicolas Barreau[a]

[a]*CNRS, Institut des Matériaux Jean Rouxel, IMN, F-44000, Université de Nantes, Nantes 44300, France*
[b]*Univ Rennes, INSA Rennes, CNRS, Institut FOTON - UMR 6082, F-35000 Rennes, France*

On the role of sodium and copper off-stoichiometry in Cu(In,Ga)S_2 for photovoltaic applications: Insights from the Investigation of more than 500 samples

Abstract

The present article discusses the investigation of $CuIn_{1-x}Ga_xS_2$ (CIGS) thin films for photovoltaic applications. For decades, a Cu-rich composition has been used to create solar cells with efficiencies of up to 13.5%; however, interest in chalcopyrite sulfide has recently been revived due to its high and adjustable bandgap, making it a serious candidate as a top cell in tandem configurations. Although chalcopyrite selenides share many properties with CIGS thin films, crucial differences have been reported. To further understand these materials, we studied more than 500 samples of absorbers and resulting solar cells. First, we found that the compositional window for obtaining single-phase CIGS thin films with a 3-stage co-evaporation process is very narrow. Second, we reported that a combination of low copper content and sodium addition during growth is required to maximize the Photoluminescence intensity (*i.e.* to minimize the absorber-related open-circuit voltage losses). Finally, we showed that solar cell performance and stability depend not only on absorber quality but also on phenomena at interfaces (absorber/buffer and grain boundaries). Altogether, we formulate growth recommendations for the manufacture of stable CIGS/CdS solar cells with state-of-the-art efficiency.

Keywords:

Cu(In,Ga)S2, sodium, chalcopyrite, solar cell

List of acronyms

GGI: gallium/(gallium+indium) composition ratio of the absorber layer
CGI: copper/(gallium+indium) composition ratio of the absorber layer
Cu-poor/Cu-rich: absorber with CGI under/over 1
q-FLS: quasi-Fermi Level Splitting
CIGS ; CIGSe ; CIGSSe: Cu-In-Ga-S, Cu-In-Ga-Se, Cu-In-Ga-S-Se absorber layer
V_{OC}: Open-circuit voltage
EDS: Energy-dispersive X-ray spectroscopy
CBM: Conduction Band Maximum
PLMax: Energy at which the PL emission is maximum
E_G: bandgap
SEM: Scanning Electron Microscope
J-V: current-voltage
EQE: External quantum efficiency
SLG: Soda Lime Glass
Na-barrier: SiN_x layer deposited between SLG and molybdenum back contact
DDT: During Deposition Treatment

PDT: Post-Deposition Treatment
J_{SC}: Short-circuit current density
Rsh: Shunt resistance
GBs: Grain boundaries

Introduction:

In the Cu-In-Ga-S chemical system, the material of interest for PV application is the one with the chalcopyrite structure[1]. In the absence of gallium, it has been reported that this phase does not tolerate deviation from the 1:1:2 ($CuInS_2$) reference composition[2,3]. Thus, a Cu/In ratio other than 1 results in a two-phase mixture. When some of the indium is replaced by gallium, chalcopyrite tolerates a small copper deficiency resulting in a $Cu_{1-z}(In,Ga)_{1+z/3}S_2$ composition. For the element III ratio used in this study (i.e. Ga/(In+Ga), later labelled GGI ≈ 0.2), this tolerance does not exceed a few percent according to a study based on powder material[4]. The copper content is thereafter discussed in terms of the CGI ratio (Cu/(Ga+In)) of the absorber layer, and the samples are referenced to as Cu-poor (CGI < 1) or Cu-rich (CGI > 1). Until recently, the highest efficiencies were achieved with Cu-rich absorber composition, with efficiency limited to ≈13% by both interface and bulk recombinations[5,6]. A low quasi-Fermi Level Splitting (q-FLS) assesses those later. Today, all reported CIGS state-of-the-art solar cell efficiencies (≈15%) are based on Cu-poor compositions[7–10]. This allows not only to improve bulk properties but also to suppress absorber/buffer interface recombination, provided the commonly used CdS buffer layer is exchanged for a material with lower electron affinity such as ZnOS, ZnSnO or ZnMgO[7,11,12] . However, the efficiency of pure sulfide CIGS solar cells remains significantly lower than that of pure selenide $Cu(In,Ga)Se_2$ (CIGSe) [13] and mixed sulfo-selenide CIGSSe[14] cells. Inferior bulk properties are the cause: Siebentritt et al[15] recently concluded that the presence of a deep defect results in low carrier lifetime, hence high Shockley-Read-Hall recombination, resulting in high non-radiative open-circuit voltage (V_{OC}) loss, and ultimately low q-FLS in comparison to the Schockley-Queisser limit. This represents now the main obstacle to achieving the level of performance required to envisage a future outside the research laboratories for sulfides CIGS. Sodium control is known to be a key factor in obtaining quality CIGSe and CIGSSe chalcopyrite solar cells as it enables high q-FLS through long photogenerated carriers lifetime[16,17]. Moreover, Herberholz et al[18] reported that for the selenide CIGSe, the chalcopyrite tolerance to copper-deficiency is widened in presence of sodium. Although this has long been suspected, the demonstration that sodium is also a key player for sulfides CIGS has only recently been provided[15], and the subject needs to be further explored in order to fully benefit from the effects associated with sodium addition.

This study focuses on two levers related to the chemistry of CIGS (copper content and sodium supply) and their effects on the material properties and the electrical parameters of the resulting solar cells. First, we modified an evaporation chamber to obtain a lateral gradient of copper content, and thus to obtain from a single deposition run a large set of samples (here 84) with varying CGI. Compared to a conventional approach (as many syntheses of absorbers as different compositions), the approach used here avoids the issues related to the reproducibility of the different synthesis steps and provides a large library of samples of different compositions in a short time. However, this requires a large number of samples to be characterised (primarily by measuring their composition) quickly and without modification. The first step was to establish a link between the CGI measured by Energy-dispersive X-ray spectroscopy (EDS) and the intensity ratio of different Raman peaks. Photoluminescence (PL) spectra are recorded immediately afterwards in the same instrument as the Raman, to evaluate the optoelectronic properties of the absorbers. Indeed, the variations of q-FLS are determined by the variations of the radiative efficiency (i.e. the intensity of the

photoluminescence) according to equation (1)[19–21] while the energy at which the PL emission is maximum (PLMax) is found to be a good approximation of CIGS bandgap. In this way, the CGI, the bandgap (E_G) and the relative q-FLS are all measured quickly and automatically from a unique device. After completion with buffer, window layers and grids, all solar cells were then characterized by current-voltage (J-V), and further analysis requiring more time on a few selected samples to answer questions related to layer morphology (cross-section Scanning Electron Microscope (SEM)) or to evaluate the level of interface recombination (External quantum efficiency (EQE) measurements with/without voltage reverse bias). To ensure comparability with literature and between samples of different bandgaps, we discuss V_{OC}-deficit = $V_{OC,SQ}$-V_{OC} rather than the V_{OC} itself ($V_{OC,SQ}$ is the theoretical highest achievable V_{OC} for a given bandgap according to Schockley and Queisser[22] for a single junction under AM1.5 illumination).

Experimental Methods

- Cu(In,Ga)S_2 absorber preparation and labelling

The Cu(In,Ga)S_2 (CIGS) films were grown onto soda-lime-glass (SLG) substrates previously covered with a 400 nm-thick molybdenum layer; these structures are those originally optimized for Cu(In,Ga)Se_2-based devices[23]. An additional SiN_x layer was applied between the SLG and Mo-layer of some samples; this layer is then referred to as “Na-barrier” as it is known to minimize drastically the diffusion of sodium species from the SLG into the CIGS film. All CIGS absorbers were grown by co-evaporation from elemental sources following a bithermal 3-stage process. The substrates temperature during the 1st-stage was 300°C and 580°C during 2nd and 3rd. Cu-poor/Cu-rich/Cu-poor transitions were followed in time by the so-called end-point-detection method[24]. Gallium and indium evaporation fluxes were equal during the 1st and 3rd stages and set so that the gallium to indium ratio (GGI) was 0.20 ± 0.02 and the films thicknesses are ≈800nm. To achieve the lateral gradient of absorbers Cu-content (ie. CGI), the evaporation source of copper was slightly tilted relative to that yielding confocal copper, indium and gallium evaporation cones onto the substrate. Additional sodium can be supplied to the absorber layer through the evaporation of NaF from a dedicated effusion cell within the co-evaporation vacuum chamber, at a deposition rate of approximately 2.5 nm/min. This can be achieved either during the deposition treatment (DDT), which lasts for the entire third stage (about 5 minutes), or after the absorber deposition is completed, during a post-deposition treatment (PDT) that lasts for 5 minutes and is performed together with an S flux at a substrate temperature of 350°C. The samples are named according to the sodium delivery methods (explicitely given in Table 1): from Na-free to Na (Substrate + DDT + PDT) for which the supply of sodium is the maximum within the frame of this study. In the absence of a sodium barrier (SiNx), the sample names contain "Substrate". A schematic representation of the process and resulting CGI gradient is presented in Figure 1.

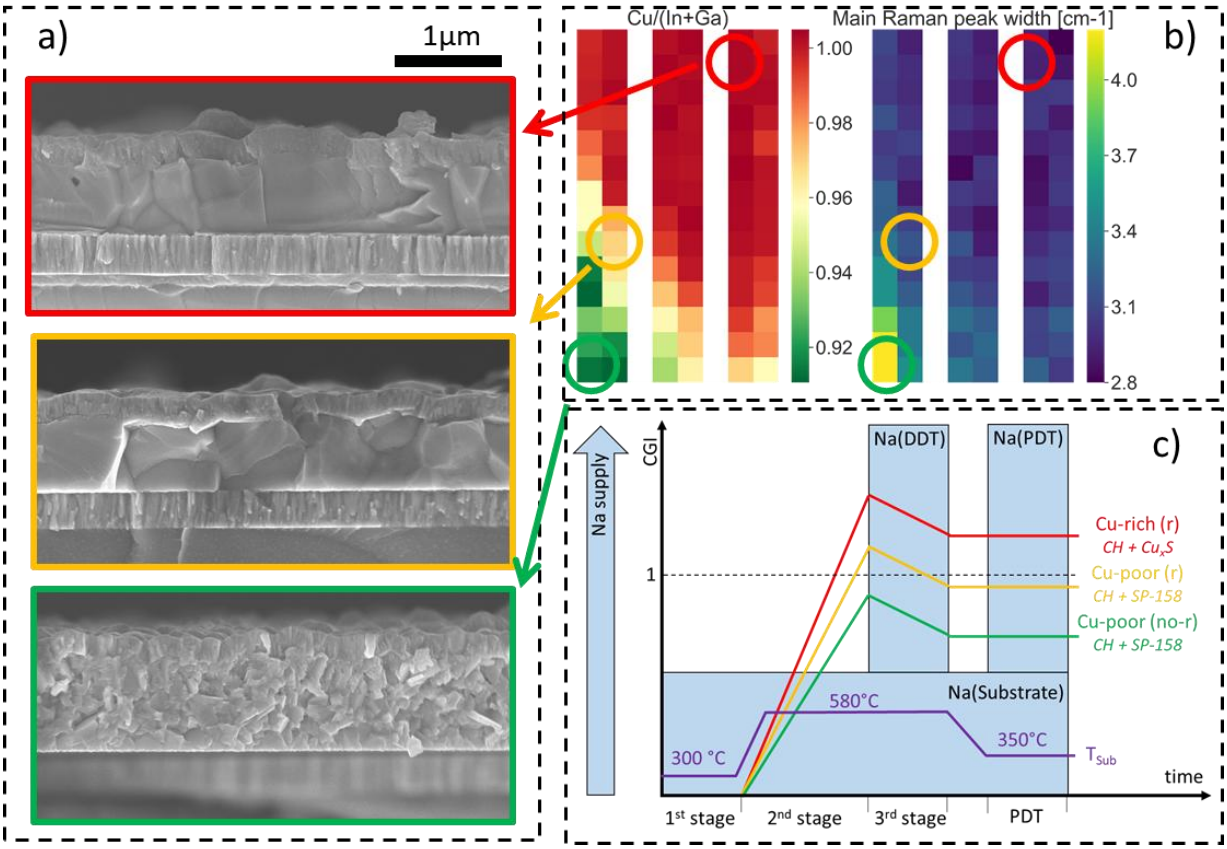

Figure 1:
a) Cross-section SEM of solar cells prepared with a (top to bottom) Cu-rich, Cu-poor recrystallized and Cu-poor not-recrystallized absorbers
b) Mappings of the same batch absorber's CGI (left) and main Chalcopyrite Raman Peak FWHM (right)
c) Schematic description of the process sequence: evolution of the substrate temperature, CGI and sodium supply over the process sequence. The time, Na-supply and CGI axis give qualitative information; CH, SP-158 = Chalcopyrite, Spinel-158 phases

Name	**Sodium supply**		
	During growth		After growth
	Substrate	DDT	PDT
Na-free	No	No	No
Na(PDT)	No	No	Yes
Na(DDT)	No	Yes	No
Na(Substrate)	Yes	No	No
Na(Substrate+PDT)	Yes	No	Yes
Na(Substrate+DDT)	Yes	Yes	No
Na(Substrate+DDT+PDT)	Yes	Yes	Yes

Table 1: Description of the sodium sources of the different samples

- Raman spectra acquisition and treatment

Raman spectra were collected on absorbers with a Renishaw inVia system, using a 514 nm Laser as an excitation source. The spectra are fitted with 8 Lorentzian curves and the CGI are determined from the intensity ratio between selected Lorentzian curves (see Figure 2 and supplementary information). No difference is observed between the composition measured on raw absorbers and after the HCl etching of finished cells (such etching removing the CdS/ZnO layers).

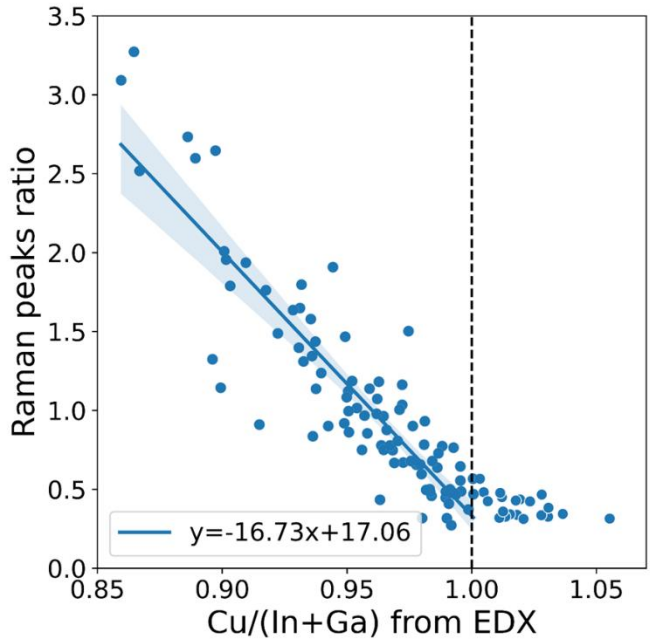

Figure 2: Correlation between intensity ratio of selected Raman peaks and EDX measured composition (full description in Supplementary Information). Linear regression is performed in the CGI <1 domain.

- Photoluminescence

Photoluminescence (PL) spectra were collected on absorbers with a Renishaw inVia system, using a 488 nm Laser as an excitation source. Spectra fit yields the PLMax and PL intensity. This later can be used to calculate Non-Radiative (NR) V_{OC} losses with respect to a reference sample. This reference sample is our sample which yields the highest PL intensity signal (*i.e.* the lowest NR losses).

$\Delta \mathrm{NRloss} = \mathrm{NRloss}_{\mathrm{sample}} - \mathrm{NRloss}_{\mathrm{ref}} = -k_b T * \ln\left(\frac{PLIntensity,sample}{PLIntensity,reference}\right)$ (equation 1), with k_b being the Boltzmann constant.

- Device preparation

All devices have CIGS/CdS/ZnO/ZnO:Al structure, deposited onto either SLG/Mo or SLG/SiNx/Mo substrates. CdS buffer layer was deposited by chemical bath deposition (CBD) following the same recipe as that described in [25]; note that all absorbers were dipped for 1 min into KCN solution (0.1 M) at room temperature. The purpose of this step is to remove the Cu_xS located on the surface of the copper-rich samples. Thus, the total composition of the copper-rich absorbers is reduced to CGI=1 (or slightly more if the etch is imperfect), that of the copper-poor absorbers is not affected. The window layer consists of 50 nm-thick ZnO covered with 250 nm-thick ZnO:Al layer RF-sputtered from ceramic

targets. Solar cells are finally completed with metallic grids (Ni/Al) deposited by e-beam across a shadow mask and devices scribed mechanically.

- Electrical characterization and V_{OC} deficit

External quantum efficiency (EQE) measurements were performed at room temperature using a laboratory-built setup. Photovoltaic parameters were extracted from J-V measurements performed under standard conditions. Partial absorber layers peeling off forces us to cut cells of different sizes ranging from 0.1 to 0.5 cm². Individual cells area being imprecisely known, we use the short-circuit current density (J_{SC}) as measured from the integrated EQE of the best cell of each run. While it tends to slightly (up to 10% relative) overestimate the efficiency of poor devices, the method gets more and more accurate as efficiency increases. To calculate the V_{OC} deficit, Schockley-Queisser V_{OC} is calculated approximating that the PLMax equals the bandgap. The difference between PLMax and bandgap extracted from EQE (minimum of the EQE derivative) on 33 solar cells is not significant (all values ≤30meV, while EQE is recorded which steps of 10nm, *i.e.* ≈20meV – see Supplementary Information).

Results and discussions

1- CIGS films physicochemical properties

As previously mentioned, the copper evaporation source was intentionally tilted to create a gradient of copper-flux from one edge of the substrates to the other (Figure 1). This flux variation was such that a narrow part of the CIGS sample did not undergo Cu-poor/Cu-rich transition, and thus did not recrystallize; the corresponding area looks much darker than the rest of the sample. Each of the specific areas, namely Cu-rich, Cu-poor recrystallized and Cu-poor not recrystallized, were observed by SEM after all analyses, cells completion and testing. Figure 1 shows representative cross-sectional views of three solar cells prepared from the same run of KCN-etched CIGS absorbers, two of which recrystallized (one Cu-rich and one Cu-poor) while not the other. Both films which have Cu-rich composition temporarily during their growth (*i.e.* films which recrystallized) have the same morphology: they are made of large grains, extended throughout the entire film thickness. The film that did not recrystallize is compact as well but made out of much finer grains. In conclusion, the size of the grains constituting the films appears driven only by the Cu-poor/Cu-rich transition; neither the final CGI (in the investigated range) nor the sodium availability during or after growth (see supplementary information) seem to affect grains size.

To investigate the influence of substrate's nature (*ie.* diverse availability of sodium) and growth specificities (*i.e.* Recrystallization or not and final CGI), Raman spectra were investigated. In fact, in addition to the detection of crystalline phases thanks to assignable peaks position, Raman peaks width increases along with the density of crystalline defects. Figure 3 plots the Full Width Half Maximum (FWHM) of the main chalcopyrite line (at 293 cm^{-1})[26] as a function of CGI. This graph shows at least two pieces of information. Firstly, the peak assigned to the chalcopyrite phase becomes narrower with increasing CGI, independently of whether the sample recrystallized or not; note that for CGI ≈1, a limit value is achieved. To better observe this trend, it is advisable to limit the analysis to samples from the same batch, due to potential batch-to-batch variations (see supplementary information). Secondly, for similar CGI, the peak width of recrystallized samples spectra is systematically much narrower than that of non-recrystallized films. These observations are

consistent with improved crystalline order with increasing CGI[27]; that is (i) copper deficiency results in higher defects density, (ii) the recrystallization phenomenon drags crystalline defects out of the grains (*i.e.* toward grain boundaries)[28].

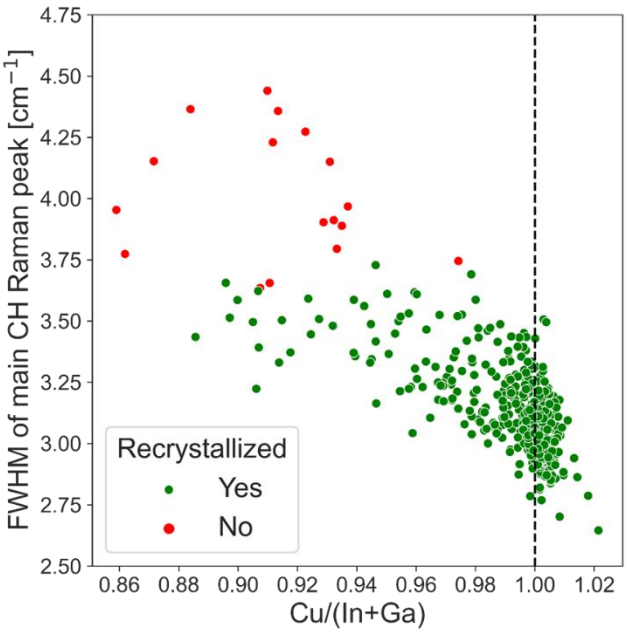

Figure 3: FWHM of the main Chalcopyrite Raman peak as a function of Cu/(In+Ga) and recrystallization

Additionally, systematic exploitation of all Raman spectra (218 in total, see more data in Supplementary Information) suggests that, in the range of investigated GGI, absorbers switch from a combination of Cu_xS + Chalcopyrite-CIGS (CH-CIGS) phases for CGI > 1, to a mix of spinel $Cu(In,Ga)_5S_8$ and CH-CIGS phases for CGI < 1[26]. As a consequence, the single-phase CH-CIGS domain is extremely narrow in those experimental conditions (thin films grown by 3-stage process). A similar observation was already reported in the case of powder samples[4]. Note that, here as well, the results of these characterizations are similar whatever the strategy for sodium-incorporation.

As a conclusion of this section, polycrystalline films resulting from the implemented 3-stage process are made of grains, which size only depends on whether they underwent Cu-rich composition relative to 1:1:2 during the synthesis, leading to recrystallization. A deviation in CGI from 1 results in the formation of either Cu_xS or the so-called 158-spinel phase as secondary phases for Cu-rich and Cu-poor compositions, respectively [4,15]. Note the same conclusions can be drawn whatever the strategy implemented to supply sodium to the film. Also none of the different sodium supply strategies appears to enhance the tolerance of the CH-CIGS sulfide for increased Cu-deficiency.

2- Absorber properties

In order to explore the impact of both CGI and the various ways to supply sodium, all samples were studied by photoluminescence spectroscopy. PL intensity gives access to quantitative estimation of non-radiative recombination variation ΔNRloss (see equation 1) compared to a reference, which in first approximation varies as q-FLS. This approximation is acceptable when E_G-PLMax does not significantly vary, which is the case here (see Supplementary Information). This measurement will therefore be used as a criterion to assess the quality of the films (most likely the doping and the

lifetime of the photogenerated carriers), as a tenfold increase in PL intensity rises the q-FLS by 60meV (equation 1). Figure 4 plots the PL intensity of the main peak versus CGI for both types of substrates (*i.e.* SLG/Mo and SLG/SiNx/Mo) and sodium addition routes (i.e. PDT and DDT). These plots show first that when the films are Cu-rich (*i.e.* CGI > 1), the PL intensity is rather low and depends neither on the nature of the substrate nor on the sodium addition strategy. Regarding Cu-poor composition, Na-free samples experience similarly low values as Cu-rich samples. Na(PDT) samples show a gain of one order of magnitude but only if their CGI is very close to unity. The addition of sodium during growth (albeit the effects are similar, NaF-DDT is more efficient than Na(Substrate)) further increases the PL Intensity of Cu-poor material and makes it CGI-independent. The fact that the supply during growth (at 580°C) is much more efficient than PDT (350°C) shows that the incorporation of sodium into the CIGS bulk requires a high temperature. We note that using the same glass, Mo and substrate temperature resulting in high-efficiency CIGSe[29], the substrate-supplied sodium is not sufficient to obtain the best quality CIGS film.

In conclusion, contrary to the morphology/crystallinity observations reported in the previous section, PL measurements show that the properties of the films are strongly dependent on whether the absorber is Cu-rich or Cu-poor, on the addition of sodium and a fortiori on the way it is supplied - DDT being the most effective. When DDT is performed, the type of substrate and PDT have no effect. The increased PL intensity difference observed, two orders of magnitudes, is expected to result in a V_{OC}-deficit improvement of as much as ≈120mV.

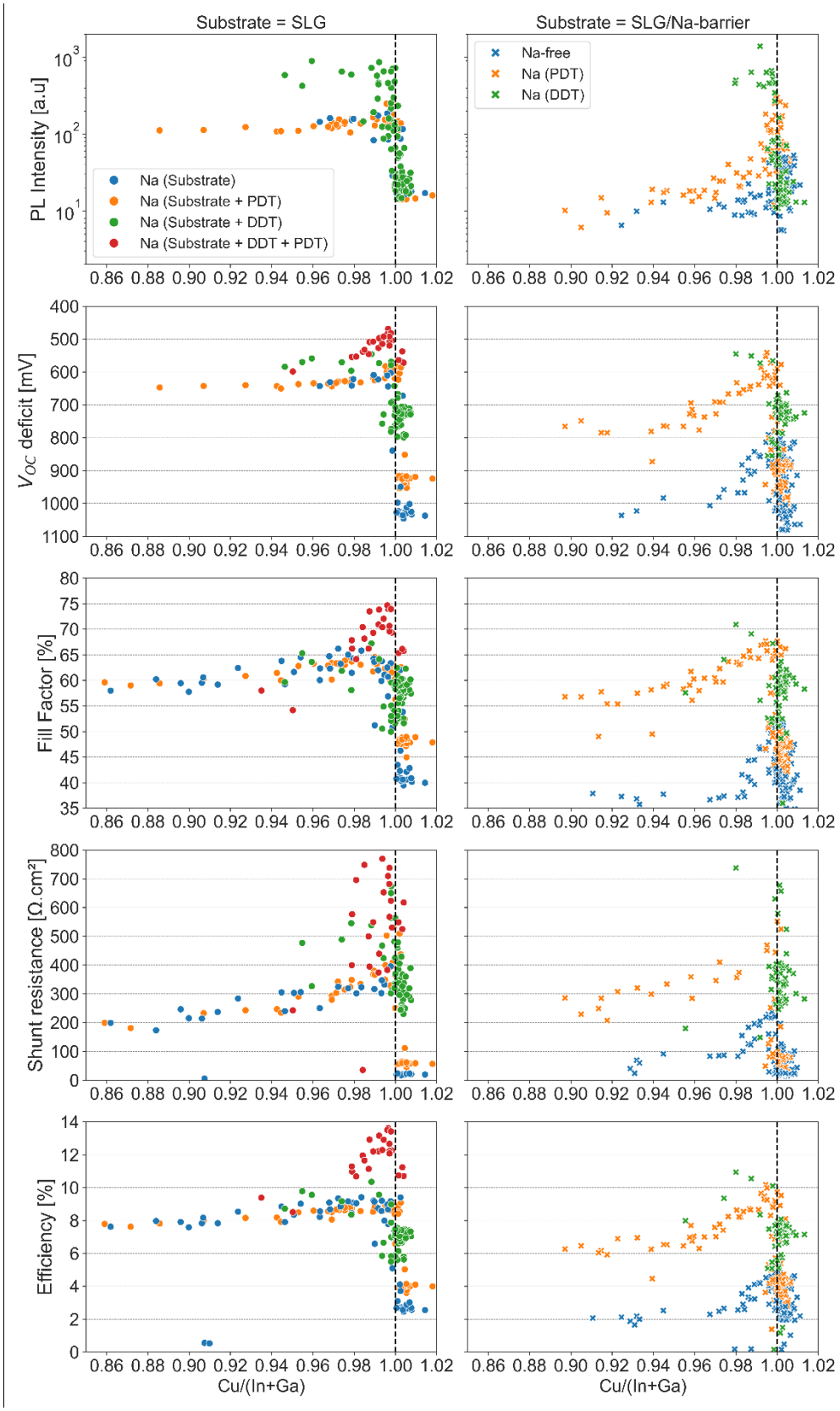

Figure 4: Optoelectronic properties as a function of the Cu/(In+Ga) composition and the sodium supply – left/right plot = SLG/Na-Barrier substrate. Blue/orange/green/red = no/PDT/DDT/PDT and DDT additional sodium supply. PL data for the for the Na(Substrate + DDT + PDT) are missing as CdS

buffer layer was deposited immediately after absorber growth in order to avoid air and laser degradation that may occur during PL measurement.

3- Solar cells properties and discussion

All CIGS films were dipped into a solution of KCN (0.1 M for 2 min) before being covered with CdS and ZnO/AZO window layer. Such KCN treatment[30,31] is known to etch Cu_xS phases as well as eventual oxides from the surface of the absorber. Consequently, the variations observed in photovoltaic parameters of the investigated devices originate from (i) remaining secondary phases, either not etched by KCN (158-spinel phase) or located at an unreached area (i.e. grain boundaries (GBs) or rear interface) (ii) and/or point and 1D crystalline defects. The following sections describe the solar cell parameters and correlate with the conclusions exposed in the previous sections. The results of cells prepared from Cu-rich absorbers will be presented before those fabricated from the Cu-poor ones. Figure 4 plots the V_{oc}-deficit of devices versus CGI for the two types of substrates and the diverse routes followed to supply the films with additional sodium.

Focusing on cells based on a Cu-rich absorber, V_{OC} deficit and FF are extremely bad without DDT (Figure 4). Surprisingly, they both significantly improve with DDT, independently of the substrate which may appear in contradiction with the conclusions of PL measurements. In fact, based on their bulk properties (PL Intensity), all so-called Cu-rich devices should have similar V_{oc}-deficit, which is obviously not the case. One explanation lies in the evolution of the shunt resistance (Figure 4), which at the same time screens the effective V_{oc} and dramatically limits the FF. DDT yields improved FF and V_{OC} through increased shunt resistance (Rsh).

Solar cells based on Cu-poor CIGS systematically perform over the Cu-rich from the same batch. Once again, Na-free processes result in the poorest properties and (Cu-poor & Na-free) devices show only slightly improved performance (Rsh, V_{OC} and FF) compared to Cu-rich unless the CGI is increased up to close to one. Unlike Cu-rich, the sodium supply via NaF-PDT or substrate already improves Rsh and makes it somewhat resilient to lower CGI values. Once again, DDT has similar but more pronounced beneficial effects. Altogether, slightly Cu-poor absorbers with DDT yield the best solar cells, and additional sodium supply via substrate does not seem to have a significant effect. The gain obtained on the Na(Substrate+DDT+PDT) batch is attributed to the processing of the full device processing straight after the absorber synthesis (hence limiting air exposure and laser induced degradation during characterizations) rather than to effect of PDT itself.

The variations described above may be explained as follows: At first, low shunt resistance values are likely due to copper-enriched grain boundaries – by analogy to CIGSe material, for which grain boundaries have been extensively studied[32–34]. Then, the addition of sodium enables excess copper out-diffusion from grain boundaries towards the surface where depending on the stage of the process it forms either CIGS or Cu_xS; in the latter case, it is subsequently etched by KCN. The fact that supplying NaF at high substrate temperature during the growth (DDT) is more efficient is consistent with this speculative explanation. Then, the FF and V_{OC}-deficit degradation observed when absorbers get further Cu-poor (whilst absorber quality (PL intensity) remains constant) tend to confirm that the presence of 158-spinel (whose amount increases as CGI moves away from 1) induces absorber/buffer interface recombination. We do observe that sodium supply results in a further decrease of the V_{OC} deficit than expected by the intrinsic properties alone. There is no doubt that this is partly due to the increase in shunt resistance, but additional phenomena may play a role. A complementary explanation could be the inclusion of sodium in the spinel $CuIn_5S_8$ phase, resulting in $(Na,Cu)In_5S_8$ at the surface of the absorber layer. This latter has a lower electron affinity than the former[35];

therefore, it likely better aligns with the chalcopyrite and CdS conduction bands[36,37] which reduces the absorber/buffer interface cliff losses. EQE measurements (see Figure 5) support this latter hypothesis. Indeed, cells prepared with Na-free, Na(PDT) and Na(DDT) absorbers with a similar Cu-poor composition experience similar EQE under 800mV reverse bias (*i.e.* similar current photo generation and collection length). When the bias is suppressed, the Na-free cells experience a strong wavelength-independent drop in the EQE, which is characteristic of significant interface recombination[38]. This feature partially/almost completely disappears with PDT/DDT respectively, demonstrating a reduction of this recombination mechanism. The best performances being obtained for compositions as close as possible to stoichiometry suggests that the (Na,Cu) 158 spinel-phase, although less deleterious than its copper-pure counterpart, remains problematic.

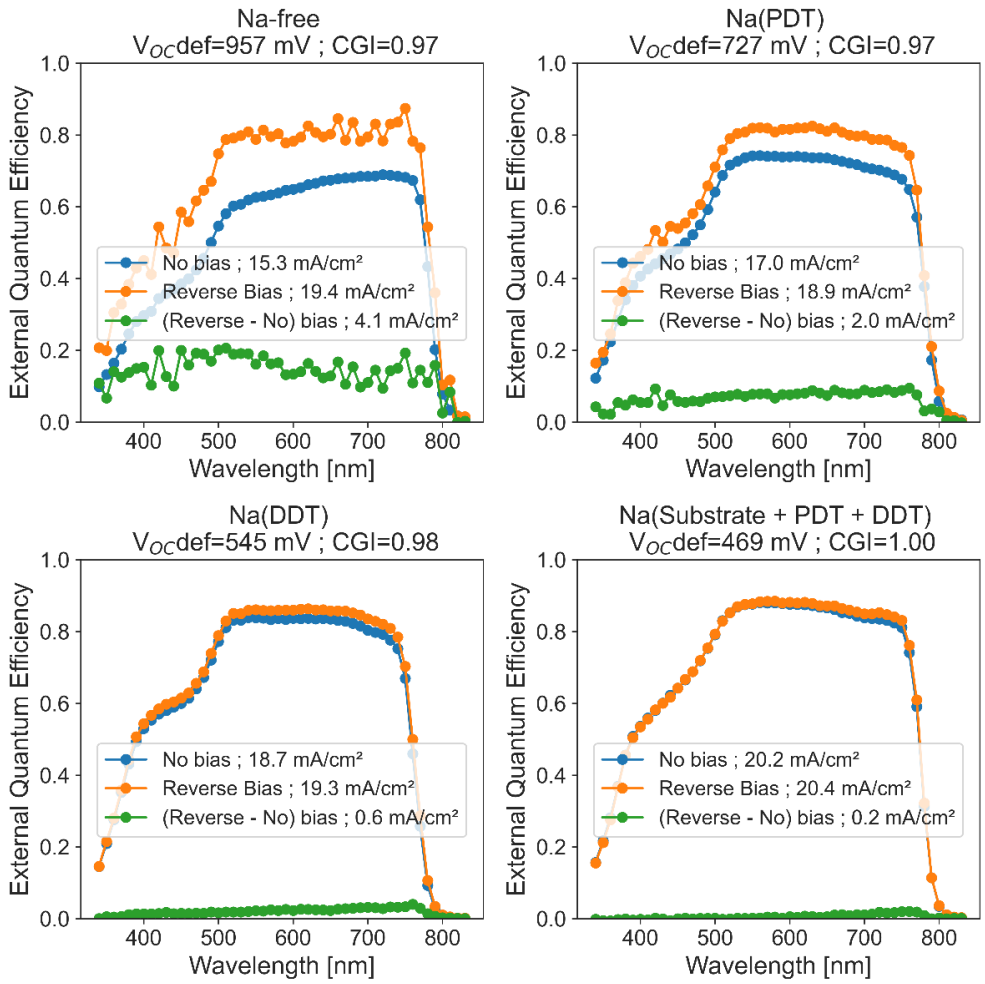

Figure 5: External quantum efficiency without(blue) and with a 800 mV reverse bias(orange). Difference between both conditions (green) for 4 different samples. Na-free, Na(PDT) and Na(DDT) slightly Cu-poor samples are display to highlight the effect of Na-addition on spinel-158 phase topped absorbers. Stoichiometric (CGI=1) Na(Substrate + PDT + DDT) is a sister-sample of the record cell.

To maximize efficiencies, the last batch of solar cells was prepared with a slightly modified procedure: absorbers were prepared with a maximized sodium supply: Na(Substrate + DDT + PDT) and the CdS buffer layer was deposited immediately after absorber growth to make sure that no air, time and laser(during PL measurement) degradation occur. This strategy effectively results in the lowest V_{OC} deficits together with the highest FF hence the best efficiencies. Since this procedure

prevents the PL measurements from being carried out, we cannot comment on the possible role of intrinsic bulk properties on the V_{OC}-deficit reduction. Nevertheless, the lowered discrepancy between EQE w/wo reverse bias compared to other processes translates into reduced interface recombination.

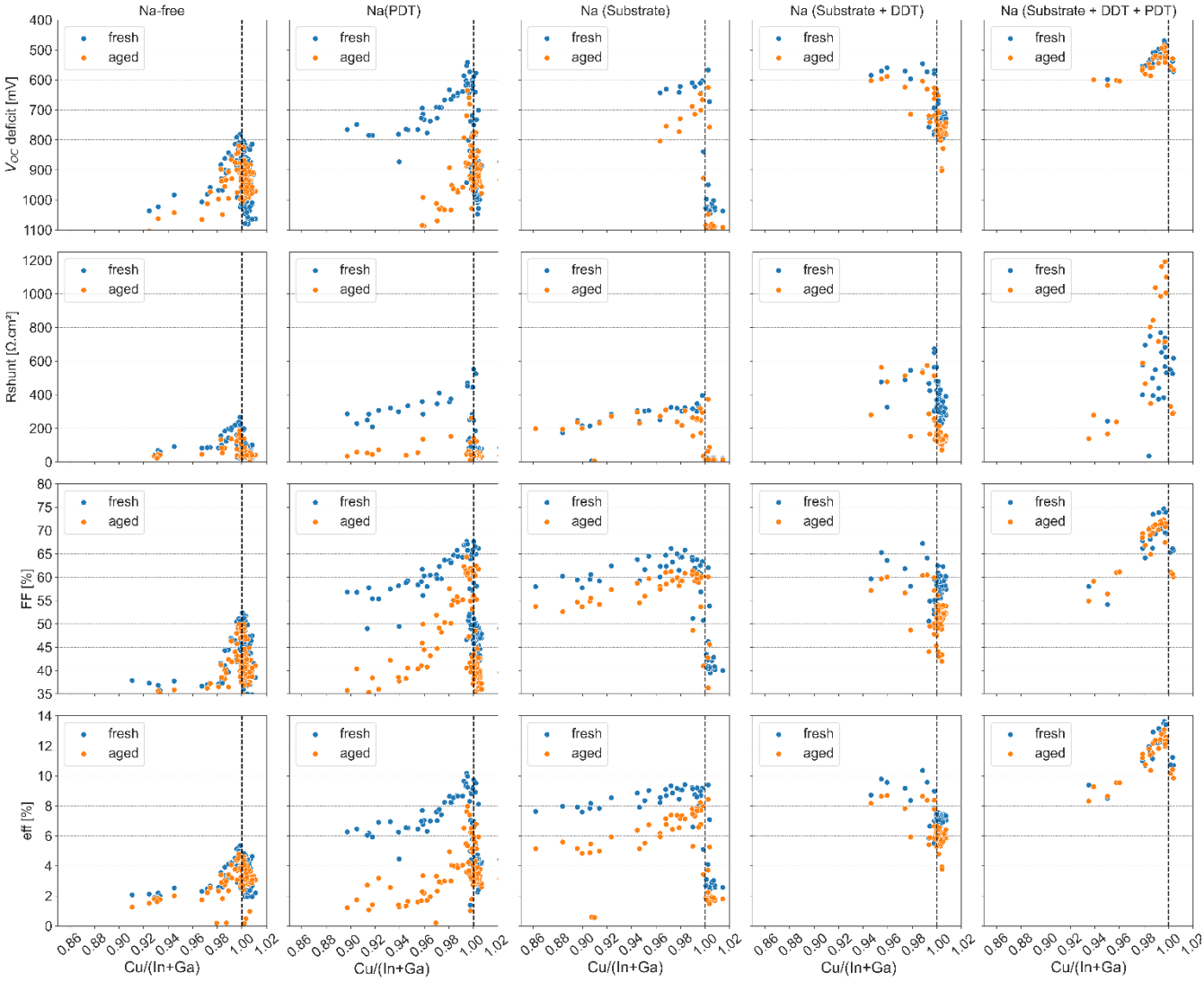

Figure 6: Evolution solar cell electrical properties before(blue)/after(orange) 3 weeks of storage in the dark

We also found that sodium influences the stability of solar cells (Figure 6). Here, the cells were stored for 3 weeks in the dark before measuring again their I-V characteristics. Although very low, performance of the Na-free cells is stable over time. Na(PDT) fresh devices, which shunt resistance was higher than Na-free, strongly degrade during the storage down to levels achieved by Na-free cells. As long as sodium is supplied during growth (by the substrate and DDT), the shunt resistance appears stable over time.

In agreement with the previous observations, and considering that copper and sodium are mobile elements, especially in the junction area (where the electric field facilitates it) one can imagine that

copper-sodium exchange mechanisms explain the observed ageing effects. In the absence of sodium during growth (Na-free and Na(PDT) samples), the bulk of the grains is Na-free. The PDT brings sodium to the grain boundaries, increasing the shunt resistance. Over time, the sodium in the grain boundaries would exchange with copper in the bulk, forming copper-rich grain boundaries and thus drastically reduce shunt resistance values down to those seen in Na-free samples. If no sodium is available (Na-free sample) or if the interior of the grain already contains sodium because of its supply during growth (by DDT and/or substrate), this mechanism would not occur thus the resistance be stable over time. When insufficient sodium is supplied during growth (Na(Substrate) and Na(Substrate+PDT) samples) both the V_{OC} deficit and FF deteriorate over time despite the shunt resistance remains similar. The problem being solved with DDT, we suggest an additional copper-sodium exchange mechanism to occur and degrade bulk or interface properties. Altogether, optimizing sodium supply does not only improve efficiency but also makes it stable over time. Our proposed explanation for this instability involves mechanisms of copper-sodium redistribution between grain boundaries, grains interior, and surface.

Table 2: Comparison of this work most efficient solar cell with literature cells
act= active area, ARC= with antireflection coating

	Buffer	E_G(eV)	V_{OC}(mV)	$V_{OC\ def}$ (mV)	FF (%)	J_{SC} (%)	η (%)
This work	CdS	1.63	884	469	74	20.8 [act]	13.6 [act]
Shukla[10]	CdS	1.6	854	472	71.6	21 [act]	12.8 [act]
Shukla[10]	ZnOS	1.6	902	424	73	23.1 [act.ARC]	15.2 [act. ARC]
Hiroi[7]	ZMO	1.57	920	378	72.2	23.4 [ARC]	15.5 [ARC]

4- Conclusions

The present study investigated the influence of copper content and sodium supply on $CuIn_{1-x}Ga_xS_2$ (CIGS) thin films for photovoltaic applications, with a focus on understanding the factors that influence the stability and efficiency of these materials. Through the analysis of more than 500 samples of absorbers and resulting solar cells, we found that the compositional window for obtaining single-phase CIGS thin films with a 3-stage co-evaporation process is very narrow, and that a combination of slightly copper-poor composition and sodium addition during growth is required to minimize absorber-related open-circuit voltage losses. In addition, we identified the formation of a copper-poor secondary phase (the spinel phase) and the presence of copper-enriched grain boundaries as detrimental to solar cell performance. Sodium supply at any time was found to yield a massive performance improvement driven by an increase in shunt resistance. We attribute it to the repel of copper excess out of the grain boundaries. Sodium supply during the growth process (through the absorber or via DDT) also improved the intrinsic properties of Cu-poor absorbers and reduced losses at the absorber/buffer interface. These findings have several implications for the design and manufacture of stable, high-efficiency CIGS solar cells. For example, our results suggest that careful control of copper content and sodium supply is critical for achieving optimal device performance, and that alternative buffer layer materials may be needed to reduce interface recombination losses. In addition, our study highlights the importance of understanding the role of interface phenomena, including the spinel phase and grain boundaries, in CIGS solar cell performance and stability, and the need for further research to clarify the mechanisms at play. Overall, our study provides new insights into the factors that influence the properties of CIGS thin

films, and represents an important step towards the development of practical, high-performance and stable photovoltaic devices based on these materials.

[1] S. Siebentritt, Chalcopyrite compound semiconductors for thin film solar cells, Curr. Opin. Green Sustain. Chem. 4 (2017) 1–7. https://doi.org/10.1016/j.cogsc.2017.02.001.

[2] J.J.M. Binsma, L.J. Giling, J. Bloem, Phase relations in the system Cu2S-In2S3, J. Cryst. Growth. 50 (1980) 429–436. https://doi.org/10.1016/0022-0248(80)90090-1.

[3] K.V. Sopiha, J.K. Larsen, J. Keller, M. Edoff, C. Platzer-Björkman, J.J.S. Scragg, Off-stoichiometry in I–III–VI2 chalcopyrite absorbers: a comparative analysis of structures and stabilities, Faraday Discuss. 239 (2022) 357–374. https://doi.org/10.1039/D2FD00105E.

[4] A. Thomere, C. Guillot-Deudon, M. Caldes, R. Bodeux, N. Barreau, S. Jobic, A. Lafond, Chemical crystallographic investigation on Cu2S-In2S3-Ga2S3 ternary system, Thin Solid Films. 665 (2018) 46–50. https://doi.org/10.1016/j.tsf.2018.09.003.

[5] R. Klenk, J. Klaer, R. Scheer, M.Ch. Lux-Steiner, I. Luck, N. Meyer, U. Rühle, Solar cells based on CuInS2—an overview, Thin Solid Films. 480–481 (2005) 509–514. https://doi.org/10.1016/j.tsf.2004.11.042.

[6] S. Merdes, R. Mainz, J. Klaer, A. Meeder, H. Rodriguez-Alvarez, H.W. Schock, M.Ch. Lux-Steiner, R. Klenk, 12.6% efficient CdS/Cu(In,Ga)S2-based solar cell with an open circuit voltage of 879mV prepared by a rapid thermal process, Sol. Energy Mater. Sol. Cells. 95 (2011) 864–869. https://doi.org/10.1016/j.solmat.2010.11.003.

[7] H. Hiroi, Y. Iwata, S. Adachi, H. Sugimoto, A. Yamada, New World-Record Efficiency for Pure-Sulfide Cu(In,Ga)S2 Thin-Film Solar Cell With Cd-Free Buffer Layer via KCN-Free Process, IEEE J. Photovolt. 6 (2016) 760–763. https://doi.org/10.1109/JPHOTOV.2016.2537540.

[8] H. Hiroi, Y. Iwata, K. Horiguchi, S. Adachi, N. Sakai, H. Sugimoto, 960mV open circuit voltage chalcopyrite solar cell, in: 2015 IEEE 42nd Photovolt. Spec. Conf. PVSC, 2015: pp. 1–4. https://doi.org/10.1109/PVSC.2015.7355655.

[9] N. Barreau, E. Bertin, A. Crossay, O. Durand, L. Arzel, S. Harel, T. Lepetit, L. Assmann, E. Gautron, D. Lincot, Investigation of co-evaporated polycrystalline Cu(In,Ga)S2 thin film yielding 16.0 % efficiency solar cell, EPJ Photovolt. 13 (2022) 17. https://doi.org/10.1051/epjpv/2022014.

[10] S. Shukla, M. Sood, D. Adeleye, S. Peedle, G. Kusch, D. Dahliah, M. Melchiorre, G.-M. Rignanese, G. Hautier, R. Oliver, S. Siebentritt, Over 15% efficient wide-band-gap Cu(In,Ga)S2 solar cell: Suppressing bulk and interface recombination through composition engineering, Joule. 5 (2021) 1816–1831. https://doi.org/10.1016/j.joule.2021.05.004.

[11] M. Sood, J. Bombsch, A. Lomuscio, S. Shukla, C. Hartmann, J. Frisch, W. Bremsteller, S. Ueda, R.G. Wilks, M. Bär, S. Siebentritt, Origin of Interface Limitation in Zn(O,S)/CuInS2-Based Solar Cells, ACS Appl. Mater. Interfaces. 14 (2022) 9676–9684. https://doi.org/10.1021/acsami.1c19156.

[12] M. Sood, D. Adeleye, S. Shukla, T. Törndahl, A. Hultqvist, S. Siebentritt, Low temperature (Zn,Sn)O deposition for reducing interface open-circuit voltage deficit to achieve highly efficient Se-free Cu(In,Ga)S2 solar cells, Faraday Discuss. 239 (2022) 328–338. https://doi.org/10.1039/d2fd00046f.

[13] P. Jackson, R. Wuerz, D. Hariskos, E. Lotter, W. Witte, M. Powalla, Effects of heavy alkali elements in Cu(In,Ga)Se2 solar cells with efficiencies up to 22.6%, Phys. Status Solidi RRL – Rapid Res. Lett. 10 (2016) 583–586. https://doi.org/10.1002/pssr.201600199.

[14] M. Nakamura, K. Yamaguchi, Y. Kimoto, Y. Yasaki, T. Kato, H. Sugimoto, Cd-Free Cu(In,Ga)(Se,S)2 Thin-Film Solar Cell With Record Efficiency of 23.35%, IEEE J. Photovolt. 9 (2019) 1863–1867. https://doi.org/10.1109/JPHOTOV.2019.2937218.

[15] S. Siebentritt, A. Lomuscio, D. Adeleye, M. Sood, A. Dwivedi, Sulfide Chalcopyrite Solar Cells—Are They the Same as Selenides with a Wider Bandgap?, Phys. Status Solidi RRL – Rapid Res. Lett. 16 (2022) 2200126. https://doi.org/10.1002/pssr.202200126.

[16] P.M.P. Salomé, H. Rodriguez-Alvarez, S. Sadewasser, Incorporation of alkali metals in chalcogenide solar cells, Sol. Energy Mater. Sol. Cells. 143 (2015) 9–20. https://doi.org/10.1016/j.solmat.2015.06.011.
[17] S. Uličná, L.M. Welch, A. Abbas, M. Togay, V. Tsai, T.R. Betts, A.V. Malkov, J.M. Walls, J.W. Bowers, Sodium doping of solution-processed amine-thiol based CIGS solar cells by thermal evaporation of NaCl, Prog. Photovolt. Res. Appl. 29 (2021) 546–557. https://doi.org/10.1002/pip.3408.
[18] R. Herberholz, U. Rau, H.W. Schock, T. Haalboom, T. Gödecke, F. Ernst, C. Beilharz, K.W. Benz, D. Cahen, Phase segregation, Cu migration and junction formation in Cu(In, Ga)Se2, Eur. Phys. J. Appl. Phys. 6 (1999) 131–139. https://doi.org/10.1051/epjap:1999162.
[19] J.K. Katahara, H.W. Hillhouse, VOC overestimation from photoluminescence quantum yield in disordered absorber layers, in: 2016 IEEE 43rd Photovolt. Spec. Conf. PVSC, 2016: pp. 3563–3566. https://doi.org/10.1109/PVSC.2016.7750335.
[20] S. Siebentritt, T.P. Weiss, M. Sood, M.H. Wolter, A. Lomuscio, O. Ramirez, How photoluminescence can predict the efficiency of solar cells, J. Phys. Mater. 4 (2021) 042010. https://doi.org/10.1088/2515-7639/ac266e.
[21] S. Siebentritt, U. Rau, S. Gharabeiki, T.P. Weiss, A. Prot, T. Wang, D. Adeleye, M. Drahem, A. Singh, Photoluminescence assessment of materials for solar cell absorbers, Faraday Discuss. 239 (2022) 112–129. https://doi.org/10.1039/D2FD00057A.
[22] Detailed Balance Limit of Efficiency of p-n Junction Solar Cells: Journal of Applied Physics: Vol 32, No 3, (n.d.). https://aip.scitation.org/doi/10.1063/1.1736034 (accessed December 21, 2022).
[23] P. Bommersbach, L. Arzel, M. Tomassini, E. Gautron, C. Leyder, M. Urien, D. Dupuy, N. Barreau, Influence of Mo back contact porosity on co-evaporated Cu(In,Ga)Se2 thin film properties and related solar cell, Prog. Photovolt. Res. Appl. 21 (2013) 332–343. https://doi.org/10.1002/pip.1193.
[24] J. Kessler, C. Chityuttakan, J. Lu, J. Schöldström, L. Stolt, Cu(In,Ga)Se2 thin films grown with a Cu-poor/rich/poor sequence: growth model and structural considerations, Prog. Photovolt. Res. Appl. 11 (2003) 319–331. https://doi.org/10.1002/pip.495.
[25] T. Kodalle, L. Choubrac, L. Arzel, R. Schlatmann, N. Barreau, C.A. Kaufmann, Effects of KF and RbF post deposition treatments on the growth of the CdS buffer layer on CIGS thin films - a comparative study, Sol. Energy Mater. Sol. Cells. 200 (2019) 109997. https://doi.org/10.1016/j.solmat.2019.109997.
[26] J.K. Larsen, K.V. Sopiha, C. Persson, C. Platzer-Björkman, M. Edoff, Experimental and Theoretical Study of Stable and Metastable Phases in Sputtered CuInS2, Adv. Sci. 9 (2022) 2200848. https://doi.org/10.1002/advs.202200848.
[27] C. Xue, D. Papadimitriou, Y.S. Raptis, N. Esser, W. Richter, S. Siebentritt, M.Ch. Lux-Steiner, Compositional dependence of Raman scattering and photoluminescence emission in CuxGaySe2 thin films, J. Appl. Phys. 94 (2003) 4341–4347. https://doi.org/10.1063/1.1605813.
[28] N. Barreau, T. Painchaud, F. Couzinié-Devy, L. Arzel, J. Kessler, Recrystallization of CIGSe layers grown by three-step processes: A model based on grain boundary migration, Acta Mater. 58 (2010) 5572–5577. https://doi.org/10.1016/j.actamat.2010.06.025.
[29] T. Lepetit, Influence of KF post deposition treatment on the polycrystalline Cu(In,Ga)Se2/CdS heterojunction formation for photovoltaic application, Theses, Université de nantes, 2015. https://hal.archives-ouvertes.fr/tel-03613348 (accessed December 21, 2022).
[30] L. Weinhardt, O. Fuchs, D. Groß, E. Umbach, C. Heske, N.G. Dhere, A.A. Kadam, S.S. Kulkarni, Surface modifications of Cu(In,Ga)S2 thin film solar cell absorbers by KCN and H2O2/H2SO4 treatments, J. Appl. Phys. 100 (2006) 024907. https://doi.org/10.1063/1.2216367.
[31] B. Canava, J.F. Guillemoles, J. Vigneron, D. Lincot, A. Etcheberry, Chemical elaboration of well defined Cu(In,Ga)Se2 surfaces after aqueous oxidation etching, J. Phys. Chem. Solids. 64 (2003) 1791–1796. https://doi.org/10.1016/S0022-3697(03)00201-4.

[32] M. Gloeckler, J.R. Sites, W.K. Metzger, Grain-boundary recombination in Cu(In,Ga)Se2 solar cells, J. Appl. Phys. 98 (2005) 113704. https://doi.org/10.1063/1.2133906.
[33] G. Sozzi, R. Menozzi, N. Cavallari, M. Bronzoni, F. Annoni, M. Calicchio, M. Mazzer, On the temperature behavior of shunt-leakage currents in Cu(In,Ga)Se2 solar cells: The role of grain boundaries and rear Schottky contact, in: 2015 IEEE 42nd Photovolt. Spec. Conf. PVSC, 2015: pp. 1–4. https://doi.org/10.1109/PVSC.2015.7355779.
[34] U. Rau, K. Taretto, S. Siebentritt, Grain boundaries in Cu(In, Ga)(Se, S)2 thin-film solar cells, Appl. Phys. A. 96 (2009) 221–234. https://doi.org/10.1007/s00339-008-4978-0.
[35] C. Guillot-Deudon, S. Harel, A. Mokrani, A. Lafond, N. Barreau, V. Fernandez, J. Kessler, Electronic structure of Na x Cu 1 − x In 5 S 8 compounds: X-ray photoemission spectroscopy study and band structure calculations, Phys. Rev. B. 78 (2008) 235201. https://doi.org/10.1103/PhysRevB.78.235201.
[36] A. Lafond, C. Guillot-Deudon, S. Harel, A. Mokrani, N. Barreau, S. Gall, J. Kessler, Structural study and electronic band structure investigations of the solid solution NaxCu1−xIn5S8 and its impact on the Cu(In,Ga)Se2/In2S3 interface of solar cells, Thin Solid Films. 515 (2007) 6020–6023. https://doi.org/10.1016/j.tsf.2006.12.044.
[37] E. Ghorbani, P. Erhart, K. Albe, Energy level alignment of Cu(In,Ga)S2 absorber compounds with In2S3, NaIn5S8, and CuIn5S8 Cd-free buffer materials, Phys. Rev. Mater. 3 (2019) 075401. https://doi.org/10.1103/PhysRevMaterials.3.075401.
[38] M. Turcu, O. Pakma, U. Rau, Interdependence of absorber composition and recombination mechanism in Cu(In,Ga)(Se,S)2 heterojunction solar cells, Appl. Phys. Lett. 80 (2002) 2598–2600. https://doi.org/10.1063/1.1467621.

Acknowledgments:

The technical staff of the laboratory are acknowledged for their precious advices and support in carrying out the experiments, in particular Jean-Yves Mevellec for the Raman spectroscopy and Nicolas Stephant for the SEM and EDS.

This was supported by the French National Agency projet PECALO (Dispositif photoélectrochimiques tandem pour la réduction du dioxyde de carbone et l'oxydation des alcools) grant no. Projet-ANR-20-CE05-0019.

This was supported by the French National Agency projet EPCIS (Cellules Tandem Epitaxiales à Haut Rendement CIGS-Silicium) grant no. Projet-ANR-20-CE05-0038.